Ultrasound of Fetal Cardiac Anomalies

Prabhakar Rajiah[1]
Ceayee Mak[2]
Theodore J. Dubinksy[3]
Manjiri Dighe[3]

OBJECTIVE. Fetal cardiac anomalies are common, with half of them being lethal or requiring complex surgeries. Early detection of these anomalies enables early referral to tertiary care centers with adequate expertise. A routine antenatal ultrasound performed between 18 and 22 weeks enables detection of most of these malformations. Further comprehensive evaluation can be performed with a dedicated fetal echocardiography, particularly in high-risk pregnancies and in cases with extracardiac anomalies.

CONCLUSION. Doppler imaging is used in the evaluation of vascular and valvular lesions. Three-dimensional imaging enables reconstruction of multiple complex planes from a single transverse acquisition. Four-dimensional imaging enables cine looping of images in multiple planes, enabling estimation of cardiac motion and function. This review illustrates the various sonographic techniques for evaluation of fetal hearts and the imaging appearance of various fetal cardiac anomalies.

Keywords: anomalies, cardiac, fetal, heart, malformations, ultrasound

DOI:10.2214/AJR.10.7287

Received September 2, 2010; accepted after revision December 3, 2010.

T. J. Dubinksy is a consultant for ConnexMD.

[1]Imaging Institute, Cleveland Clinic, 9500 Euclid Ave, Cleveland, OH 44195. Address correspondence to P. Rajiah (radprabhakar@gmail.com).

[2]Kaiser Foundation Hospital, The Permanente Medical Group, San Francisco, CA.

[3]Body Imaging Department, University of Washington Medical Center, Seattle, WA.

CME
This article is available for CME credit.
See www.arrs.org for more information.

WEB
This is a Web exclusive article.

AJR 2011; 197:W747–W760

0361–803X/11/1974–W747

Congenital cardiac disease is seen in 2–6.5 of 1000 live births and is a major cause of morbidity and mortality, with half of these cases being lethal or requiring surgical correction. Environmental, genetic, and chromosomal abnormalities are believed to be causes of congenital cardiac defects, with a higher incidence among infants with affected siblings or mother. Extracardiac abnormalities are associated with 25% of these cases [1, 2].

Detection of cardiac anomalies can be challenging and is typically done by fetal cardiac ultrasound performed between 18 and 22 weeks. Transvaginal scan can detect anomalies even at 12–13 weeks. Detailed fetal echocardiography is performed in high-risk cases, which could be a result of fetal (extracardiac anomalies, increased nuchal translucency, hydrops, or polyhydramnios), maternal (teratogen exposure, metabolic disorders, congenital heart defect, folic acid deficiency, or autoantibodies), or familial (sibling or father with congenital heart defect and Mendelian syndromes) factors. Detection of anomalies alters the obstetric course and outcome, including reassurance, termination, fetal therapy, mode of delivery, and postnatal referral to a tertiary care center with advanced expertise in management of these patients [2].

This review illustrates the imaging techniques and imaging appearance of various fetal cardiac anomalies seen with various sonographic techniques.

Fetal Cardiac Ultrasound

The first step in fetal cardiac ultrasound is to evaluate the orientation of the fetus within the maternal abdomen—that is, fetal laterality (presentation and lie). Orientation is assessed from a transverse section of the fetal abdomen. If the fetal head is found below this level and the spine is posterior, then the left side of the fetus should be located on the right side of the maternal abdomen and the stomach should be on this side (Fig. 1A). On the other hand, if the fetal head is found above this level and the spine is posterior, then the right side of the fetus is located on the right side of the maternal abdomen and the stomach is located on the opposite side [3] (Fig. 1B).

Situs is the position that an organ occupies in relation to the bilateral body symmetry. For atrial situs, this is the relationship of the atria with respect to each other. This is conventionally established by noting the arrangement of the aorta and inferior vena cava (IVC) at the level of the diaphragm, because great vessel arrangement is similar to thoracic and atrial

situs. In situs solitus, the IVC is anterior and to the right of the aorta (Fig. 2A). In situs inversus, there is a mirror image pattern, with the aorta to the right of the IVC (Fig. 2B). In situs ambiguous, the aorta and IVC are located on the same side of the spine in right isomerism (Fig. 2C) and the aorta is centrally located, with an interrupted IVC in left isomerism [3] (Fig. 2D).

Views in Fetal Cardiac Ultrasound

The basic view performed in cardiac ultrasound is the four-chamber view [4], which can detect 43–96% of fetal anomalies [1]. "Extended basic views" of the left ventricular outflow tract (LVOT) and right ventricular outflow tract (RVOT) increase the sensitivity for the detection of anomalies. Alternatively, a comprehensive set of five short-axis projections can be acquired.

The four-chamber view is obtained by a transverse projection through the fetal thorax above the level of the diaphragm, either apical (parallel to the interventricular septum) or subcostal (perpendicular to the interventricular septum). This view shows the two atria and ventricles along with atrioventricular (AV) valves (mitral and tricuspid) and septa (interventricular and interatrial) (Fig. 3). The cardiac position and axis are determined in this projection. In levocardia, the heart is located within the left chest, with the apex pointing to the left; in dextrocardia, it is located within the right chest with the apex pointing to the right; and in mesocardia, it is centrally located with the apex pointing anteriorly. In dextroposition, the heart has a normal left-sided axis but is displaced to the right. The cardiac axis is calculated from a line drawn from the posterior spine to the anterior sternum (spinosternal line). The ventricular septum typically intersects this line at 40–45°. Cardiac axis may be altered in intracardiac conditions (Ebstein anomaly and tetralogy of Fallot) or extracardiac conditions causing mass effect or as a result of accompanying pulmonary hypoplasia [5].

Cardiac anatomy is typically evaluated using a sequential segmental approach, which depends on morphologic identification of the atria, ventricles, and great arteries, not on their spatial relationship [3]. The morphologic right atrium (RA) has a triangular appendage, whereas the morphologic left atrium (LA) has a hook-shaped appendage. Differences between the morphologic right ventricle (RV) and the left ventricle (LV) are listed in Table 1 [5]. The tricuspid valve opens into the RV and the mitral valve opens into the LV, with the septal leaflet of tricuspid valve inserting more apically than the mitral valve. Occasionally, valves may be imperforate, common, straddling, or overriding. The AV junction is the continuation of atria with the ventricular chamber. In the typical biventricular connection, each atrium connects with a ventricular chamber, which could either be concordant (i.e., RA-RV and LA- LV), discordant (i.e., RA-LV and LA-RV), or ambiguous (i.e., isomeric RA or LA with RV to the right or left of LV). In univentricular connection, one or two atrial chambers connect with a single ventricular cavity [3]. There are two arterial valves, the aortic and pulmonary, which connect the LV to the aorta and the RV to the pulmonary artery (PA), respectively. Ventriculoarterial connections can be concordant (i.e., aorta from LV and PA from RV), discordant (i.e., aorta from RV and PA from LV), double outlet (i.e., > 50% of each great artery connected to same ventricular cavity), and single outlet (i.e., only one arterial trunk connected to the ventricle).

The LVOT view is obtained by a 45° tilt of the transducer from the four-chamber view perpendicular to the septum, to an oblique plane from the fetal upper left quadrant of the abdomen to the fetal right shoulder. The aorta originates from the LVOT (Fig. 4A) and distally gives off the great vessels of the head and neck. Membranous septum is also visualized in this view. The RVOT view can be obtained by further rotation in the same direction and gentle rocking of the transducer from the LVOT view. The PA is seen exiting from the RV (Fig. 4B), dividing into the right PA and left PA (Fig. 4C) and continuing as the ductus arteriosus, which opens into the descending thoracic aorta (Fig. 5). The ascending aorta is seen centrally, wrapped by the RV and PA. In both of these projections, a normal aorta and PA are perpendicular to each other. Further rightward rotation results in short-axis views of the ventricles and thorax. Further rotation toward the left fetal shoulder shows the aorta as a central circle draped by the PA anteriorly and to the left. Rotation from the left shoulder to the right hemithorax shows the aortic arch and its branches (Fig. 5A) and ductus arteriosus (Fig. 5B). The ductal arch (RVOT, PA, and ductus arteriosus) is broader and flatter than the aortic arch.

A comprehensive set of five short-axis projections can also be acquired, with the ventricular septum parallel to the ultrasound beam. These views are better at detection of conotruncal abnormalities that are missed by the routine views. From caudad to cephalad, these views are the abdomen at the level of the stomach to identify situs; the four-chamber view; the five-chamber view, which includes a centrally placed aorta; PA bifurcation, with the PA originating from the RV located on the left side and crossing the aorta to lie to the left side and anterior of aorta; and the three-vessel view, which includes the main PA, ascending aorta, and superior vena cava (SVC) from the left anterior to the right posterior aspect of the thorax [5] (Fig. 6). The SVC typically opens into the RA (Fig. 5C) but the SVC can be bilateral, with the left SVC entering the coronary sinus. Pulmonary veins typically drain into the LA, but anomalous veins can drain into systemic veins, either partially or totally [3] (Fig. 5D).

Measurements

The cardiac chambers and vascular structures are measured and can be compared with normalized charts. The RV and LV typically are of the same size, with a 1:1 ratio. The cardiothoracic ratio is the ratio between the cardiac and thoracic circumferences, which

TABLE 1: Differences Between the Morphologic Right and Left Ventricles on Prenatal Ultrasound

Characteristic	Right Ventricle	Left Ventricle
Apical trabeculations	Coarse	Smooth
Septomarginal trabeculations	Present	Absent
Moderator band	Present	Absent
Chordal attachment to septum	Present from tricuspid valve	Absent, mitral valve has no attachment to septum
Insertion on ventricular septum	Tricuspid inserts lower	Mitral valve has normal insertion
Fibrous continuity	Absent between tricuspid and pulmonary valves	Present between mitral and aortic valves
Foramen ovale flap	Open from right atrium	Opens into the left atrium

normally measures 0.5 [6]. Volumes can be measured from 2D ultrasound using the Simpson rule, which assumes that the cross-section of each ventricular slice is cylindric and that the total volume is the sum of all cylinders. These measurements are plotted against gestational age (as determined by measurement of biparietal diameter or fetal length). Normalized charts at various gestational ages exist for the RV:LV ratio, LV wall thickness, septal wall thickness, left atrial dimension, PA diameter, and aortic root diameter. A small heart is seen as a result of hypoplasia (LV or RV or both) or of compression from extrinsic masses, whereas a large heart can be seen in various congenital abnormalities, pericardial effusion, aneurysms, cardiomyopathies, or tumors. The PA diameter is typically larger than the aorta by approximately 10%. However, as a general rule, the two can be considered to be similar in size and any discrepancy in size should be concerning.

M-Mode Ultrasound

M-mode ultrasound is a 2D image of motion over time that is used for evaluation of fetal heart motion, heart rate, wall thickness, chamber size, and motion of the valves or myocardium. Fetal heart rate and rhythm can be evaluated using M-mode ultrasound through the atrial and ventricular wall, above and below the AV valve, respectively. Chamber size and function are evaluated by focusing at the level of AV valves [6]. AV concordance can be evaluated by using M-mode ultrasound through both atrium and ventricle at the same time. Normal fetal heartbeats are 175 beats/min at 8 weeks, 140 beats/min at 20 weeks, and 130 beats/min at term [5], with a regular 1:1 AV rhythm [5].

Color-Flow, Pulsed Doppler, and Doppler Tissue Imaging

Color Doppler can be used to detect vascular flow through cardiac chambers, vascular structures, and septal defects. It also significantly reduces the time required for Doppler examination of the heart, because interrogation of vascular structures becomes easier [1]. The direction of the flow can be established, which is useful in the detection and quantification of regurgitation and stenosis. Reversal of the flow through a valve indicates regurgitation. The presence of aliasing in color Doppler indicates high velocities suggestive of stenosis. If pulsed Doppler is applied at this point, high velocity with spectral broadening can be seen. Normal peak velocity through the AV valves is 30–60 cm/s throughout gestation, and that through the arterial valves is 25 cm/s at 12 weeks and 60–100 cm/s by term [6]. Color Doppler is also used in the evaluation of pulmonary and systemic venous connections and small septal defects. Color Doppler tissue imaging has been used recently for evaluating high-amplitude low-velocity signals, such as within the moving myocardium. This can be used to encode the direction of myocardial motion, which is particularly useful in the assessment of arrhythmias [7].

Three- and Four-Dimensional Ultrasound

In 3D ultrasound, volumetric data are acquired from a single window using few seconds of scanning, which are subsequently used for reconstruction of multiple views in any plane. This reduces the overall scanning time and operator and window dependence, in addition to improving the assessment of cardiac anatomy. Planes that are not accessible in 2D scanning, such as the interventricular septum or coronal plane, can be reconstructed. Volume-rendered or surface-shaded images give an illusion of depth, which might be useful in the detection of complex anomalies, such as those involving the conotruncal septum. Alternatively, the images can be displayed as three or four simultaneous multiplanar reformatted projections with the ability to move through the volumes. Three-dimensional quantitative measurements are more accurate and reproducible than 2D techniques. Acquisition of temporal information with cardiac gating enables display of these images as cine loops in multiple planes (4D imaging), which is useful in the evaluation of cardiac motion, cardiac function, valvular function, volumes, and cardiac output. Three-dimensional imaging of regurgitation and stenotic jets is possible when 3D ultrasound is combined with color or power Doppler imaging. Three-dimensional color-flow angiography can reveal complex cardiovascular anatomy, anomalous vessels, and small septal defects [7].

Ventricular Septal Defect

Ventricular septal defect (VSD) is the most common congenital heart disease, seen in 1.5–3.5 per 1000 live births, and accounting for 30% of all cardiac anomalies [8]. The defect is most commonly (80%) seen in the membranous septum and less commonly in the muscular, outlet, or inlet portions. Defects can be variable in size. VSD is best seen in a four-chamber view as discontinuity in the ventricular septum, particularly the inlet defects. The ventricular septum is ideally evaluated in images acquired perpendicular to the interventricular septum (Fig. 7) because a pseudo-VSD, as a result of signal drop-out, can be seen in the superior aspect of images parallel to the ultrasound beam [8]. Membranous septum is also seen in the LVOT view. Outlet defects are best seen when the transducer is angled anteriorly [3]. Small defects can be difficult to detect, particularly in the perimembranous portion, but Doppler imaging can show flow across the defect. In isolated VSD, bidirectional shunting with right-to-left shunt during systole and left-to-right shunting in diastole is seen, but in VSD associated with other anomalies, unidirectional shunting may be seen. Small defects may close, but large defects require surgical closure.

Atrial Septal Defect

Atrial septal defect (ASD) is characterized by defect in a portion of the atrial septum. It is the fifth most common congenital heart disease, seen in 1 of 1500 live births [1], and is caused by abnormal tissue resorption and deposition during development of the atrial septum. According to its location, it is classified as ostium secundum (midatrial septum), ostium primum (lower atrial septum) (Fig. 8), sinus venosus (outside the atrial septum in the wall separating the SVC or IVC from the LA), and coronary sinus defect, which can be partial or complete. ASD may be difficult to visualize in a fetus because of the presence of foramen ovale. However, with high-resolution ultrasound, the septum primum is seen in the four-chamber view as a circular or linear structure with a loose pocket configuration, and the septum secundum is seen as a thick stationary structure with the foramen ovale opening into it. Normal foramen ovale measures almost same as the aortic root, with the difference being 1 mm or less [1] (Fig. 3B). The foraminal flap of the foramen ovale is seen moving into the LA at twice the heart rate. A secundum defect is seen as a larger defect in the central portion of the atrial septum or a deficient foramen flap. A primum defect is seen in the lower part of the atrial septum (Fig. 8).

AV Septal Defect

AV septal defect (AV canal defect or endocardial cushion defect) is caused by failure of fusion of the endocardial cushion, resulting in defects of the atrial ostium primum,

the ventricular inlet septum common AV valve, and the biventricular AV connections. AV septal defect accounts for 2–7% of congenital heart defects and is seen in 0.19–0.56 per 1000 live births [8]. It is associated with trisomy 21 syndrome, left atrial isomerism, hypoplastic left heart, pulmonary stenosis, coarctation, tetralogy, complete heart block, and extracardiac anomalies. There are two types: the complete type (97% of cases), with common valvular orifice, and the incomplete type, with separate right and left valve orifices. The valve of common AV junction has five leaflets, which are separate in the complete type, but two leaflets are connected by narrow tissue in the incomplete type. It is associated with a cleft in the anterior mitral leaflet. Free regurgitation is seen across the common AV valve [8]. Direct shunting may be seen from the LV into the RA. In severe forms, all four chambers communicate, causing left-to-right and right-to-left shunt. Ultrasound shows a defect in the endocardial cushion, with an inlet VSD and primum ASD (Fig. 8) associated with a single abnormal AV valve that has a T-shaped arrangement. Color Doppler shows open flow across the defect and abnormal AV valve.

Tetralogy of Fallot

Tetralogy of Fallot is characterized by narrowing of the RVOT, VSD, overriding aorta, and right ventricular hypertrophy. It accounts for 5–10% of congenital cardiac defects and is seen in 0.24–0.56 per 1000 live births [8]. It is caused by anterior displacement of the conotruncus, resulting in unequal division of conus into a small anterior RV portion and large posterior LV portion. The incomplete closure of the septum results in aortic overriding. It is associated with chromosomal and extracardiac abnormalities. On ultrasound, the aorta is seen straddling a large membranous VSD (Fig. 9). Depending on the size of the PA, it may not be easily seen and the normal crossing of aorta and pulmonary arteries is not seen. The aorta may be dilated, and the pulmonary valve is stenosed or atretic with a dilated PA. Because of the presence of normal fetal shunts, RV hypertrophy is not seen in the fetus.

Truncus Arteriosus

Truncus arteriosus is characterized by a single arterial trunk that feeds the systemic pulmonary circulation and coronary arteries with a single semilunar valve. It accounts for 1–2% of congenital cardiac defects, is seen in 0.08–0.16 per 1000 live births [8], and is caused by failure of fusion and descent of the conotruncal ridge. It almost always straddles a VSD and receives blood from both the ventricles but rarely originates almost completely from the RV or LV. There are four types (Collett Edwards classification) based on the level of origin of the aorta and pulmonary arteries [9]. An admixture of oxygenated and deoxygenated blood in the common trunk results in subnormal systemic oxygenation. The ductus arteriosus is not necessary for systemic flow and therefore does not fully develop. On ultrasound, a single arterial trunk is seen overriding the interventricular septum, with an associated VSD, and there are several branches connecting with the aorta and pulmonary vasculature (Fig. 10).

Transposition of Great Arteries

Transposition of great arteries is characterized by the abnormal origin of the great arteries from the ventricles because of abnormal spiraling of the conotruncal septum. It is broadly divided into D and L types. D-transposition accounts for 80% of transpositions and is characterized by the aorta originating from the morphologic RV and the PA originating from the morphologic LV. The pulmonary and systemic circulations operate in parallel, rather than serial, circuits. Oxygenation of systemic blood requires mixing via ASD, VSD, or patent ductus arteriosus. On ultrasound, the morphologic RV is located on the right side of the morphologic LV. The artery originating from the morphologic RV (i.e., aorta) gives off branches to the head and neck, whereas the artery originating from the morphologic LV (i.e., PA) bifurcates and there is a sharp angle of the left PA with the ductus, giving the classic "baby bird beak" sign. The aorta and PA do not cross but are parallel to each other (Fig. 11), with the aorta anterior and to the right of the PA [5].

In congenitally corrected transposition (L-transposition), in addition to the ventriculoarterial concordance, there is also AV discordance with the morphologic LA connected to the morphologic RV and the morphologic RA connected to the morphologic LV. L-transposition accounts for 1% of congenital heart defects and may be associated with VSD and pulmonic stenosis. Ultrasound shows parallel aorta and PA with the aorta anterior and to the left of the PA. The tricuspid valve may be deformed and inferiorly displaced. Differentiating this from D-transposition of great arteries requires identification of the morphologic RV and LV.

Single Ventricle

Single ventricle is characterized by a single or two AV valves opening into a single ventricle. It accounts for 2% of congenital heart defects and is caused by failure of development of the interventricular septum. The single ventricle may be the morphologic LV (85%) or the RV. The ventricle may not have an outflow tract. It may be associated with VSD, ASD, common atrium, pulmonary stenosis, and cardiosplenic syndromes. Ultrasound shows a single ventricle without an interventricular septum. Differential diagnosis includes large VSD or hypoplastic RV or LV [1].

Double Outlet RV

Double outlet RV (DORV) is characterized by the origin of more than 50% of both the aorta and PA from the RV and is caused by abnormal spiraling of the truncus arteriosus and the arrest of membranous septal formation. It accounts for less than 1% of congenital heart defects and is seen in 0.08–0.16 per 1000 live births [8]. There are four types of DORV: aorta parallel to the PA and to its right (64%), which resembles tetralogy of Fallot; aorta anterior and to the right of the PA (26%), resembling D-transposition of great arteries; aorta anterior and to the left of the aorta (7%), resembling L-transposition of great arteries; and aorta posterior and to the right of the PA (3%). DORV is almost always associated with VSD, which provides the only outlet from the LV. It is associated with maternal diabetes or alcohol intake and other cardiac defects, such as LV hypoplasia, mitral valve stenosis or atresia, aortic valve stenosis, aortic coarctation or interruption, and coronary artery anomalies. DORV is best seen in short-axis views, where the aorta and pulmonary arteries do not cross and both the vessels arise from the RV and are parallel to each other (Fig. 12). Demonstration of the origin of both the vessels from the same side of ventricular septum is essential to differentiate DORV from transposition of great arteries [8].

Hypoplastic Right Heart Syndrome

Hypoplastic right heart syndrome is characterized by an underdeveloped right side of the heart, including the RV, tricuspid valve, pulmonary valves, and PA. It is seen in 1.1% of stillbirths and is rarer than the hypoplastic left heart syndrome. It is caused by decreased blood flow in and out of the RV during development (tricuspid atresia or pulmonary atresia). The most common cause is pulmonary atresia with an intact ventricular septum. Coronary arterial supply may be abnormal.

Prenatal ultrasound shows a small RV (Fig. 13) with hypertrophy and a small or absent PA, with decreased or absent flow through the tricuspid valve and pulmonary valve [1].

Hypoplastic Left Heart Syndrome

Hypoplastic left heart syndrome is characterized by hypoplastic left-sided cardiac structures, including the LV, mitral valve, aortic valve, and aorta. It accounts for 2–4% of congenital cardiac defects and is seen in 0.16–0.25 per 1000 live births [8]. It is more common in boys and is caused by decreased flow in and out of the LV during development (e.g., mitral or aortic stenosis or atresia). Blood flow to the systemic circulation (coronary arteries, brain, liver, and kidneys) in these patients is dependent on flow through the ductus arteriosus. It is associated with aortic coarctation in 80% of cases [10]. On ultrasound, the LV is small (LV:RV ratio < 1) in size (Fig. 14); the ventricular septum makes an angle of 90° with the spinosternal line, and the aortic outflow is smaller than the pulmonary outflow tract. Mitral and aortic valves are hypoplastic or atretic. A single area of flow is seen at the AV level and bidirectional flow at the proximal aorta because of distal aortic coarctation [1].

Aortic Coarctation or Hypoplasia

Coarctation is discrete narrowing of the aortic arch, most commonly distal to the left subclavian artery. It accounts for 7% of all congenital cardiac defects [11] and 6% of cardiac anomalies seen prenatally [12]. It can be associated with chromosomal abnormalities, maternal diabetes, bicuspid valve, aortic stenosis, Turner syndrome, intracranial aneurysms, VSD, ASD, Shone complex, transposition, Taussig-Bing anomaly, and aortic hypoplasia. Coarctation may be difficult to visualize in ultrasound and is diagnosed when the distal arch is smaller than normalized values. In hypoplasia, the entire arch is small (Fig. 15). In addition, the ascending aorta is small (ratio of the PA to the ascending aorta, > 2 SD above normal). The LV can be small when it is part of the hypoplastic LV syndrome. Coarctation may progress in utero [1].

Aortic Atresia or Stenosis

Aortic stenosis is narrowing of the LVOT that can be seen at the valvular, supravalvular, or subvalvular level, with an incidence of 5.2% in newborns [1]. Valvular stenosis may be associated with chromosomal abnormalities and bicuspid aortic valve, subvalvular stenosis with hypertrophic cardiomyopathy or inherited disorders, and supravalvular stenosis with William syndrome. Ultrasound diagnosis is difficult and may show thickening of the aortic valve leaflets, with hypertrophied LV and dilated aorta as a result of poststenotic dilation. Doppler ultrasound shows high velocities across the valve (Fig. 16) and helps differentiate it from atresia.

Pulmonary Stenosis

Pulmonary stenosis can be seen at the valvular level or at the infundibulum. It is seen in 7.4% of newborns [1] and is associated with Noonan syndrome, maternal rubella, ASD, supravalvular aortic stenosis, tetralogy, and anomalous pulmonary vein return. Ultrasound diagnosis is difficult and may show thickening of the pulmonary valve leaflets, with hypertrophied RV and dilated PA as a result of poststenotic dilation. Doppler shows high velocities across the valve (Fig. 17) and differentiates it from atresia.

Ebstein Anomaly

Ebstein anomaly is characterized by displacement and attachment of one or more tricuspid leaflets (usually septal or posterior leaflets) toward the apex of the RV. The RV is divided into an "atrialized" portion above the leaflets and a muscular portion below the leaflets. It accounts for less than 1% of congenital heart defects, occurs at a rate of 7% in the fetal population, and occurs in 1 per 20,000 live births [1]. It is associated with maternal lithium use, chromosomal abnormalities, ASD, patent foramen ovale, and pulmonary stenosis or atresia. Ultrasound shows apical displacement of the tricuspid valve into the RV, tethered leaflets, reduction in the size of the functional RV (Fig. 18), increase in the size of the RV (including the atrialized portion), and tricuspid regurgitation. Cardiomegaly, hydrops, and tachyarrhythmias may be seen. Intrauterine mortality is as high as 85%. Differential diagnosis includes Uhl anomaly, tricuspid valve dysplasia, and idiopathic RA enlargement [1].

Anomalous Pulmonary Venous Return

Anomalous pulmonary venous return can be total or partial. In total anomalous pulmonary venous return, all of the pulmonary veins drain into the RA or a systemic venous channel, which then drains into the RA. This can be at supracardiac, cardiac, or infracardiac levels. In partial anomalous pulmonary venous return, there is abnormal drainage of one to three pulmonary veins directly into the systemic venous circulation. It most commonly affects the left upper lobe (47%), followed by the right upper lobe (38%), right lower lobe (13%), and left lower lobe (2%) [13]. It is bilateral in 4% of cases and is associated with sinus venosus defect in 42% of cases. Ultrasound shows lack of visibility of the four pulmonary veins entering the LA. A small atrium, dilated RV and PA, and right-to-left flow ratio greater than 2.0 are suggestive of anomalous veins.

Ectopia Cordis and Pentalogy of Cantrell

Ectopia cordis is characterized by a heart located outside the thoracic cavity. The heart can be seen in the thoracic (60%), abdominal (30%), thoracoabdominal (7%), or cervical (3%) locations [1]. Pentalogy of Cantrell is a congenital malformation caused by a continuous anterior defect in thoracoabdominal wall as a result of developmental failure of the mesoderm between 14–18 days gestational age, resulting in lower sternal defect, anterior diaphragmatic defect, parietal pericardial defect, omphalocele, and congenital cardiac anomalies, with or without ectopia cordis [14] (Fig. 19). It is usually sporadic, with variable expression. Prognosis depends on the severity of the cardiac and extracardiac malformations [14].

Cardiac Neoplasms

Cardiac neoplasms are uncommon in the fetus, with most of them being primary rather than metastastic [15]. Approximately 50% of masses are intracavitary, with inflow or outflow obstruction; 10% of these masses are malignant [1]. Rhabdomyoma (60%), teratoma (25%), fibroma (12%), hemangioma, and hamartoma are the common masses [16]. Myxoma, oncocytic cardiomyopathy, lymphangioma, metastasis, epithelial cysts, mesothelioma of AV node, and valvular blood cysts are rare [15]. Rhabdomyoma is a sessile, smooth, lobulated, and round tumor that is homogeneously echogenic (Fig. 20). It is more commonly multiple and typically located in the ventricular septum, atrial, or ventricular free walls. Rhabdomyomas usually do not cause hemodynamic compromise, grow because of maternal hormones, and spontaneously regress after birth. Multiple rhabdomyomas are associated with tuberous sclerosis in 100% and solitary tumors in 50% of cases. Rhabdomyosarcoma, however, appears clus-

tered, irregular, or fragmented. Teratoma can also originate from the pericardium or within the heart. Solid and cystic areas with foci of calcification can be seen. Pericardial effusion is always seen in these cases. Fibroma is less common and is seen as a smooth homogeneous mass that blends with the myocardium, often indistinguishable from rhabdomyosarcoma. It is commonly seen in the interventricular septum and less commonly in the ventricular free walls [15]. It is heterogeneous if there is cystic degeneration or calcification [16]. It may be associated with Beckwith-Wiedemann syndrome or Gorlin syndrome

Cardiomyopathies

Cardiomyopathies account for 8–11% of fetal cardiovascular abnormalities with one third of fetuses dying in utero [17]. Cardiomyopathies can be broadly classified as dilated, hypertrophic, and restrictive types. Intrinsic causes of primary cardiomyopathy are single-gene disorders (Noonan syndrome, familial cardiomyopathy, and metabolic abnormalities), mitochondrial and storage disorders, chromosomal abnormalities, and α-thalassemia. Extrinsic causes are intrauterine infections, maternal diseases (autoantibodies and diabetes), and twin-twin transfusion syndrome. Dilated cardiomyopathy is the end result of various cardiac disease processes and is characterized by the dilation of cardiac chambers and the reduction of systolic function (Fig. 21). In hypertrophic cardiomyopathy, the LV-RV myocardial thickness is increased (Fig. 22), without an underlying structural abnormality. It has been associated with maternal diabetes and often regresses during the first 6 months of life. Ventricular hypertrophy can also be seen because of increased afterload. Decreased LV compliance results in cardiac and respiratory distress. Restrictive cardiomyopathy is characterized typically by normal ventricular size and systolic function, but abnormal diastolic function and elevated filling pressure. Secondary cardiomyopathies have better prognosis than do idiopathic or familial cases [18].

Endocardial fibroelastosis is the most common type of restrictive cardiomyopathy and is characterized by diffuse ventricular endocardial thickening caused by proliferation of elastic and collagen fibers and occasional calcifications, predominantly involving the LV. It is sporadic, but can be familial in 10% of cases. It can be primary (infections, autoimmune, ischemia, impaired lymphatic drainage, carnitine deficiency, and mucopolysaccharidosis) when there are no structural cardiac anomalies or secondary to a structural cardiac anomaly (aortic stenosisor atresia, coarctation, mitral valve disease, anomalous coronary arteries, or VSD). In the initial stages, the LV is dilated with hypokinesis, but eventually, the LV chamber size decreases with increased wall thickness and echogenicity (Fig. 23). Tricuspid regurgitation is one of the earliest findings [1]; 80% of children with endocardial fibroelastosis present with congestive heart failure during the first year of life [19].

Echogenic Intracardiac Foci

Echogenic intracardiac foci is seen in 3–4% of fetal hearts, more commonly in the LV (93%) than the RV (5%), representing the reflection of the ultrasound waves off the small papillary muscle or chorda tendinae. It is usually insignificant but may be associated with chromosomal anomalies, such as trisomy 13 or 21, where papillary muscles or chordae may be calcified (Fig. 24). It is seen in 13–18% of children with Down syndrome [20]. Detection of echogenic intracardiac foci increases the likelihood of Down syndrome from 1.8% to 2.8% [21]. Calcification can also be seen in cardiac neoplasms, but neoplastic calcifications are larger, multiple, and not as echogenic as the echogenic intracardiac foci.

Arrhythmia

Fetal arrhythmias are seen in 2% of cases [5]. Premature atrial and ventricular contractions account for 75% and 8% of fetal arrhythmias, respectively. Premature contractions (Fig. 25A) are typically benign but may be associated with structural heart disease [1]. Arrhythmias are significant only when they are sustained (< 10%), resulting in supraventricular tachycardia (Fig. 25B) or severe bradyarrhythmia causing complete heart block. Fetal tachycardia is diagnosed when the heart rate is greater than 180 beats/min. Supraventricular tachycardia (paroxysmal supraventricular tachycardia, atrial flutter, or atrial fibrillation) is more common than ventricular tachycardia, may be associated with structural cardiac disease and hydrops fetalis, and may require medications with careful fetal and maternal monitoring. Fetal bradycardia is diagnosed when the heart rate is less than 100 beats/min, lasting more than 10 seconds, and is often associated with fetal hypoxia or asphyxia. Complete heart block may be a result of complex cardiac malformation in the AV junction or by autoimmune disorders [22].

MRI

The role of fetal MRI as a complementary tool to ultrasound in fetal imaging has grown exponentially since the first reports in 1985 [23, 24]. Unlike ultrasound imaging, this modality is not affected by maternal and fetal conditions such as obesity and oligohydramnios [25], which particularly impair sonographic visualization of the fetal heart; maternal obesity increases the rate of suboptimal ultrasound visualization of the fetal cardiac structures by 49.8% [26], despite advanced ultrasound equipment.

Recent studies have described the potential role of fetal MRI in the evaluation of the anatomy and pathology of the cardiovascular system [27, 28]; however, most studies as of yet had only healthy fetuses in their study population. The most efficient technique to characterize the fetal cardiac anatomy, according to the literature, appears to be T2-weighted true fast imaging with steady-state precession sequence, whereas the most suitable technique to evaluate the fetal cardiac function is with real-time cine-MRI.

Conclusion

Routine fetal cardiac ultrasound using four-chamber and outflow-tract views enables the detection and characterization of most of the cardiac anomalies. A further comprehensive evaluation can be performed with fetal echocardiography, particularly in high-risk pregnancies and extracardiac anomalies. Doppler imaging is used in the evaluation of vascular and valvular lesions. Three-dimensional imaging enables reconstruction of multiple complex planes from a single transverse acquisition. Four-dimensional imaging enables cine looping of images in multiple planes, enabling estimation of cardiac motion and function. MRI is a complementary tool, especially when fetal cardiac structures are visualized suboptimally with ultrasound.

References

1. Stamm ER, Drose JA. The fetal heart. In: Rumack CA, Wilson SR, Charboneau WJ, eds. *Diagnostic ultrasound*, 2nd ed. St. Louis, MO: Mosby, 1998:1123–1159
2. Small M, Copel JA. Indications for fetal echocardiography. *Pediatr Cardiol* 2004; 25:210–222
3. Carvalho JS, Ho SY, Shinebourne EA. Sequential segmental analysis in complex fetal cardiac abnormalities: a logical approach to diagnosis.

Ultrasound Obstet Gynecol 2005; 26:105–111

4. International Society of Ultrasound in Obstetric and Gynecology. Cardiac screening examination of the fetus: guidelines for performing the "basic" and "extended basic" cardiac scan. *Ultrasound Obstet Gynecol* 2006; 27:107–113
5. Naderi S, McGahan JP. A primer for fetal cardiac imaging: a stepwise approach for 2-D imaging. *Ultrasound Q* 2008; 24:195–206
6. Allan L. Technique of fetal echocardiography. *Pediatr Cardiol* 2004; 25:223–233
7. Sklanksy M. Advances in fetal cardiac imaging. *Pediatr Cardiol* 2004; 25:307–321
8. Barboza JM, Dajani NK, Glenn LG, et al. Prenatal diagnosis of congenital cardiac anomalies: a practical approach using two basic views. *RadioGraphics* 2002; 22:1125–1138
9. Collett RW, Edwards JE. Persistent truncus arteriosus: a classification according to anatomic types. *Surg Clin North Am* 1949; 29:1245–1270
10. Hawkins JA, Dody DB. Aortic atresia: morphologic characteristics affecting survival and operative palliation. *J Thorac Cardiovasc Surg* 1984; 88:620–626
11. Kimura-Hayama ET, Melendez G, Mendizabal AL, et al. Uncommon congenital and acquired aortic diseases: role of multidetector CT angiography. *RadioGraphics* 2010; 30:79–98
12. Allan LD, Crawford DC, Anderson RH, et al. The spectrum of congenital heart disease detected echocardiographically in prenatal life. *Br Heart J* 1985; 54:523–526
13. Ho ML, Bhalla S, Bierhals A, Gutierrez F. MDCT of partial anomalous pulmonary venous return in adults. *J Thorac Imaging* 2009; 24:89–95
14. Gao Z, Duan QJ, Zhang ZW, Ying LY, Ma LL. Pentalogy of Cantrell associated with thoracoabdominal ectopia cordis. *Circulation* 2009; 119: e483–e485
15. Isaacs H. Fetal and neonatal cardiac tumors. *Pediatr Cardiol* 2004; 25:252–273
16. Lacey SR, Donofrio MT. Fetal cardiac tumors: prenatal diagnosis and outcome. *Pediatr Cardiol* 2007; 28:61–67
17. Pedra SRFF, Smallhorn JF, Ryan G, et al. Fetal cardiomyopathies: pathogenic mechanisms, hemodynamic findings, and clinical outcome. *Circulation* 2002; 106:585–591
18. Yinon Y, Yagel S, Hegesh J, et al. Fetal cardiomyopathy: in utero evaluation and clinical significance. *Prenat Diagn* 2007; 27:23–28
19. Trastour C, Bafghi A, Delotte J, et al. Early prenatal diagnosis of endocardial fibroelastosis. *Ultrasound Obstet Gynecol* 2005; 26:303–306
20. Bromley B, Lieberman E, Shipp TD, Richardson M, Benacerraf BR. Significance of an echogenic intracardiac focus in fetuses at high and low risk for aneuploidy. *J Ultrasound Med* 1998; 17:127–131
21. Nyberg DA, Souter VL, El-Bastawissi A, Young S, Luthhardt F, Luthy DA. Isolated sonographic markers for detection of fetal Down syndrome in the second trimester of pregnancy. *J Ultrasound Med* 2001; 20:1053–1063
22. Kleinman CS, Nehgme RA. Cardiac arrhythmias in the human fetus. *Pediatr Cardiol* 2004; 23:234–251
23. McCarthy SM, Filly RA, Stark DD, Callen PW, Golbus MS, Hricak H. Magnetic resonance imaging of fetal anomalies in utero: early experience. *AJR* 1985; 145:677–682
24. Mazouni C, Gorincour G, Juhan V, Bretelle F. Placenta accreta: a review of current advances in prenatal diagnosis. *Placenta* 2007; 28:599–603
25. Benacerraf BR. Examination of the second-trimester fetus with severe oligohydramnios using transvaginal scanning. *Obstet Gynecol* 1990; 75: 491–493
26. Hendler I, Blackwell SC, Bujold E, et al. The impact of maternal obesity on mid trimester sonographic visualization of fetal cardiac and craniospinal structures. *Int J Obes Relat Metab Disord* 2004; 28:1607–1611
27. Gorincour G, Bourlière-Najean B, Bonello B, et al. Feasibility of fetal cardiac magnetic resonance imaging: preliminary experience. *Ultrasound Obstet Gynecol* 2007; 29:105–110
28. Chung T. Assessment of cardiovascular anatomy in patients with congenital heart disease by magnetic resonance imaging. *Pediatr Cardiol* 2000; 21:18–26

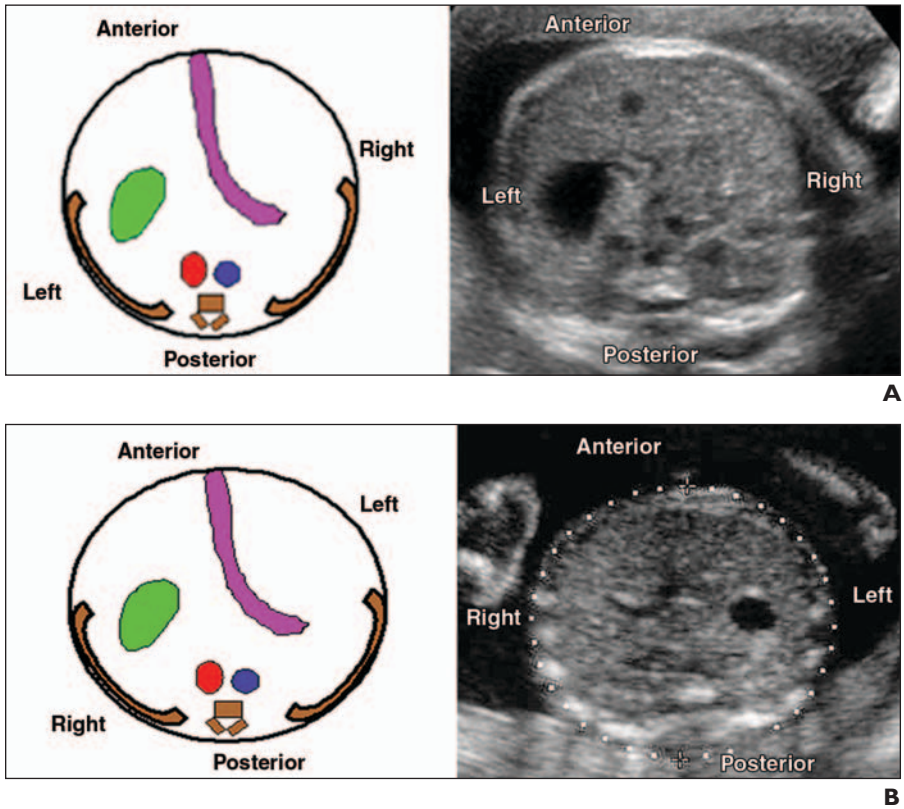

Fig. 1—Establishing laterality. Schematic diagram and ultrasound through abdomen show spine and stomach.
A, In this fetus, fetal head was located below plane of abdomen (vertex presentation), making left side lower; hence, stomach was located on left side of fetus.
B, In this fetus, fetal head was located above plane of abdominal image, making left side upper; hence, stomach was located on right side of fetus.

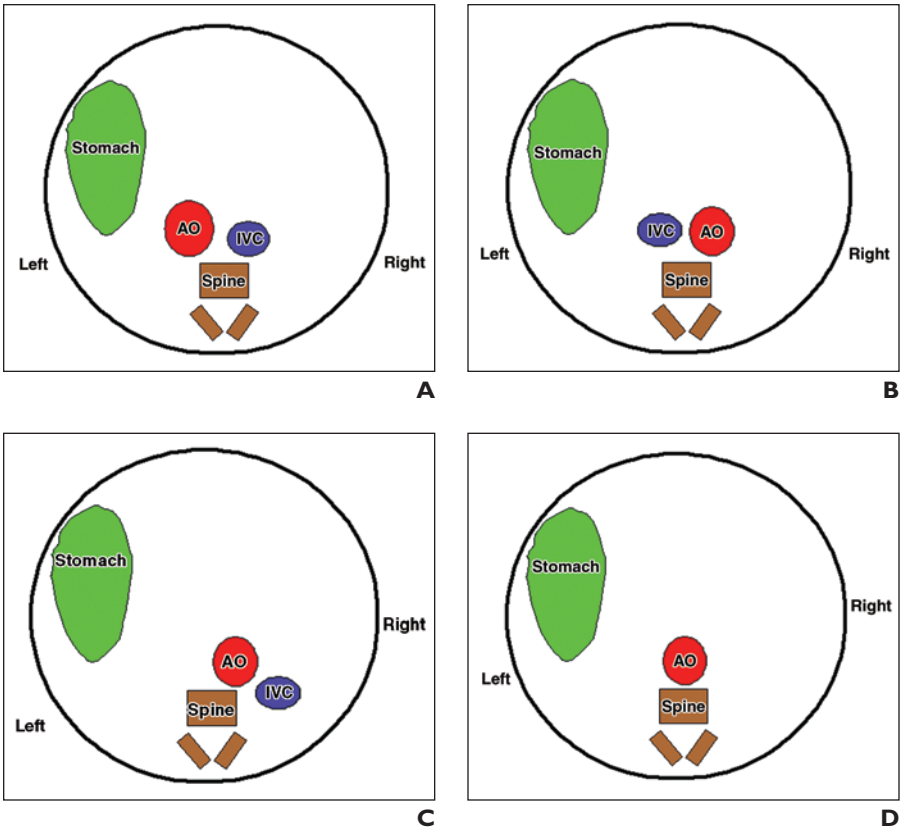

Fig. 2—Establishing situs and atrial arrangement. Diagrams represent axial images acquired at level of lower thoracic spine.
A, In situs solitus, aorta (AO) is located to left of inferior vena cava (IVC).
B, In situs inversus, AO is located to right of IVC.
C, In right isomerism, AO and IVC are located on same side of spine.
D, In left isomerism, AO is located centrally, and IVC is not visualized because it is interrupted.

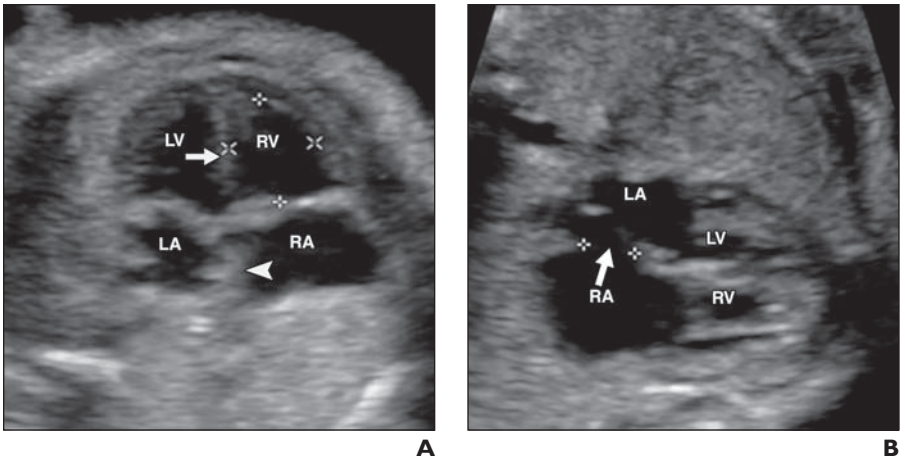

Fig. 3—Standard cardiac view.
A, Basic four-chamber view, which shows right ventricle (RV), left ventricle (LV), right atrium (RA), and left atrium (LA). Interventricular septum (*arrow*) is also seen in this view that is acquired perpendicular to ultrasound beam. Interatrial septum (*arrowhead*) is visualized.
B, Four-chamber view in another fetus shows patent foramen ovale (*arrow*).

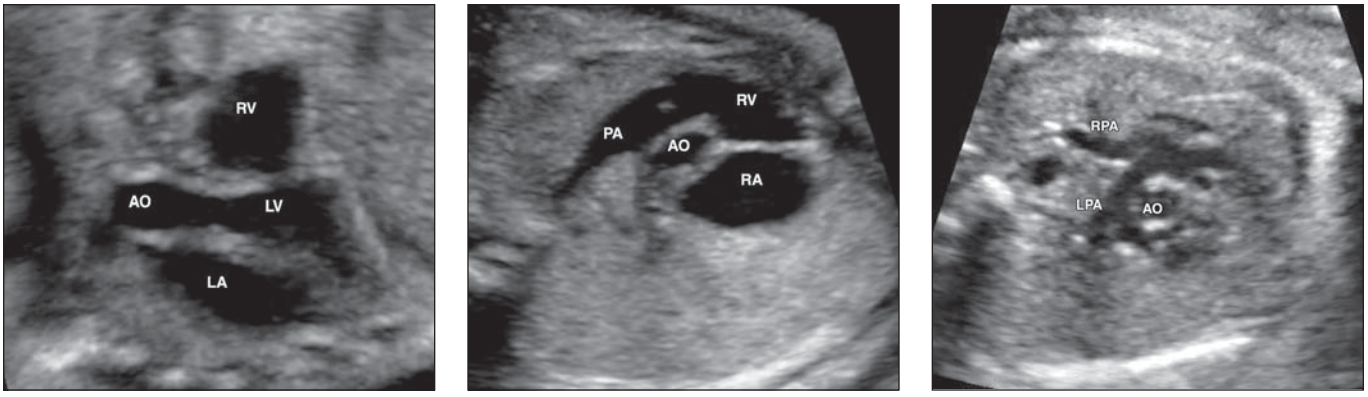

Fig. 4—Extended cardiac views.
A, Left ventricular outflow tract view shows left ventricle (LV), which gives origin to ascending aorta (AO). Right ventricular (RV) outflow tract and left atrium (LA) are also seen.
B, Right ventricular outflow tract view shows RV, giving origin to main pulmonary artery (PA). AO is seen as circular structure and is perpendicular to PA.
C, Further superiorly, right pulmonary artery (RPA) and left pulmonary artery (LPA) are seen.

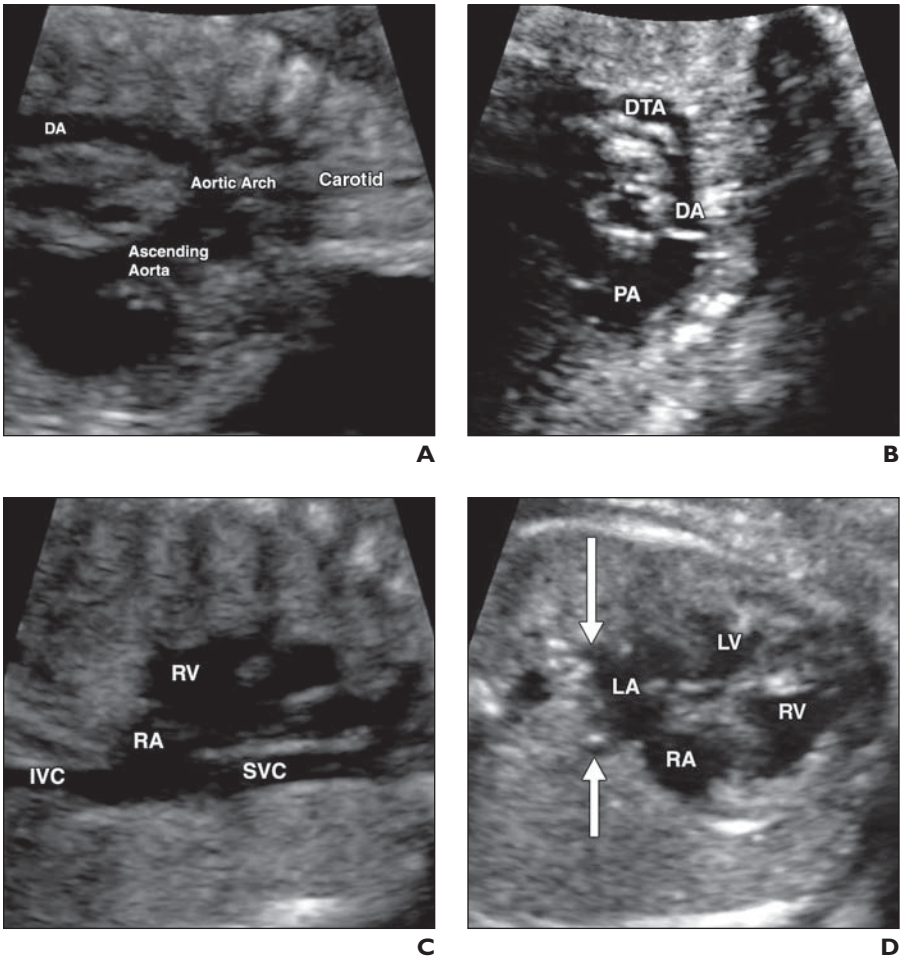

Fig. 5—Vascular structures.
A, Aortic arch can be seen giving off branches to head and neck and continuing as descending thoracic aorta (DTA). DA = ductus arteriosus.
B, DA connects pulmonary artery (PA) to DTA.
C, Superior vena cava (SVC) and inferior vena cava (IVC) open into morphologic right atrium (RA). RV = right ventricle.
D, Pulmonary veins (*arrows*) open into morphologic left atrium (LA). LV = left ventricle.

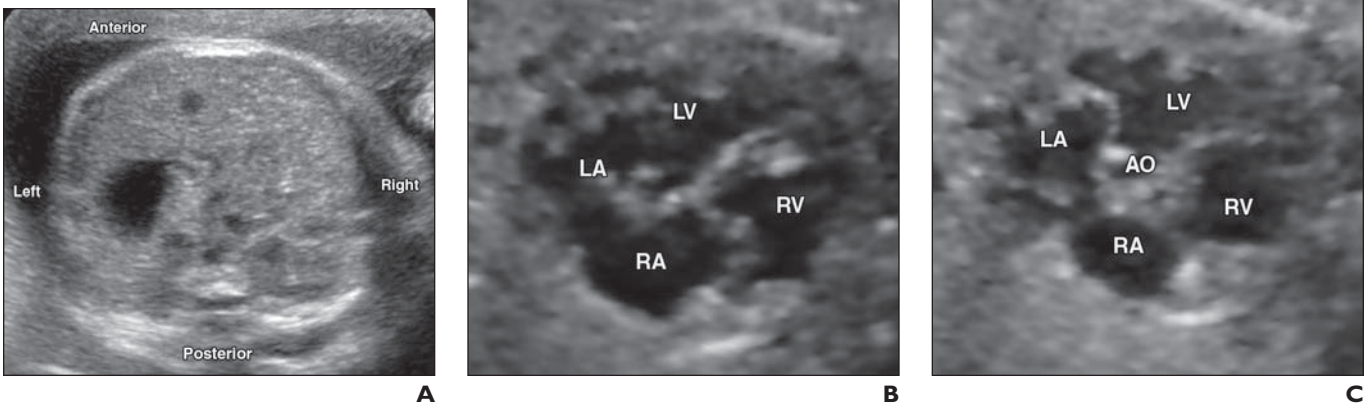

Fig. 6—Five short-axis views of heart.
A, First view is acquired in abdomen at level of stomach to identify situs.
B, Four-chamber view shows all chambers and valves. LA = left atrium, LV = left ventricle, RA = right atrium, RV = right ventricle.
C, Five-chamber view acquired just cephalad to four-chamber view shows centrally placed aorta (AO) in addition to chambers.
D, With continued cephalad motion, pulmonary artery (PA) bifurcation is seen with PA originating from RV located on left side and crossing centrally located AO to lie to left side and anterior of AO.
E, Further cephalad motion shows three-vessel view, which shows main PA, ascending AO, and superior vena cava (SVC) from left anterior to right posterior aspect of thorax.

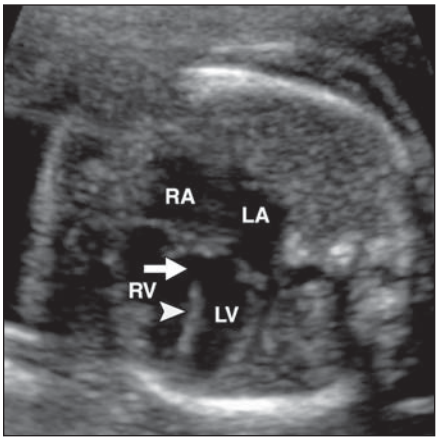

Fig. 7—Ventricular septal defect. Four-chamber view shows small defect (*arrow*) in inlet portion of interventricular septum (*arrowhead*). LA = left atrium, LV = left ventricle, RA = right atrium, RV = right ventricle.

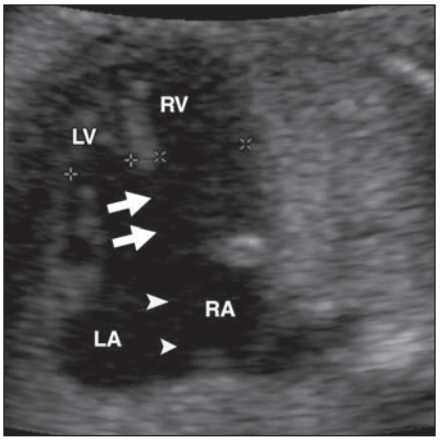

Fig. 8—Atrioventricular canal defect. Four-chamber view shows large defect in inlet part of interventricular septum (*arrows*) and complete absence of interatrial septum (*arrowheads*), with free communication of all cardiac chambers, consistent with atrioventricular septal defect. LA = left atrium, LV = left ventricle, RA = right atrium, RV = right ventricle.

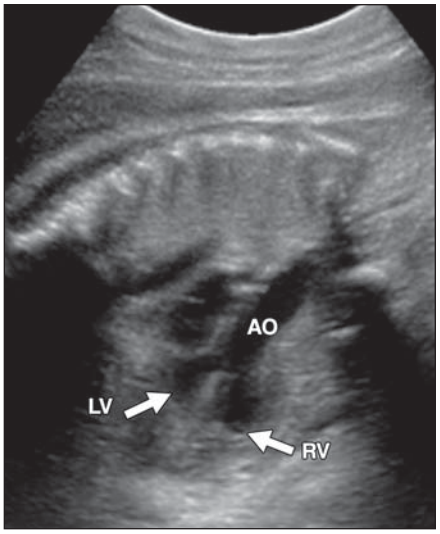

Fig. 9—Tetralogy of Fallot. Outflow tract view shows aorta (AO) overriding ventricular septal defect (*arrows*). Pulmonary artery was visualized separately (not shown). These findings are consistent with tetralogy of Fallot. LV = left ventricle, RV = right ventricle.

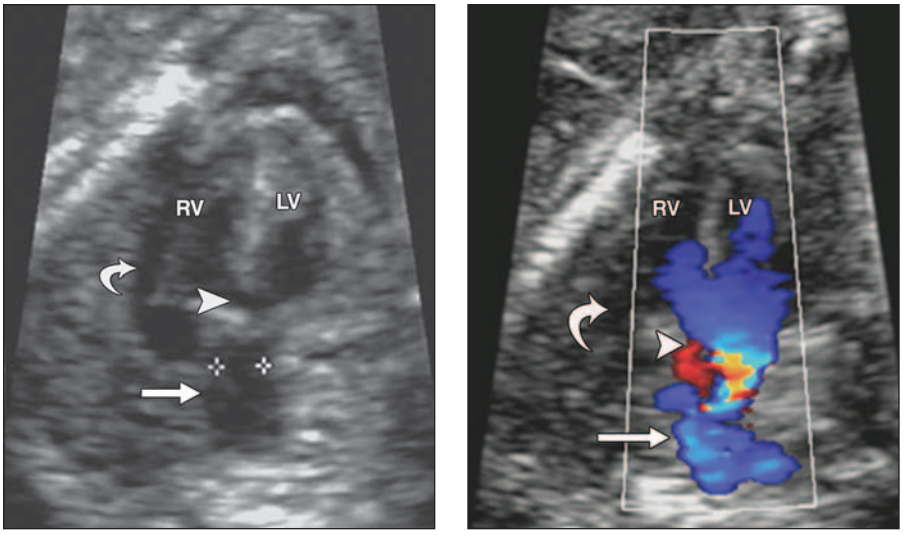

Fig. 10—Truncus arteriosus.
A, Outflow tract view shows common arterial trunk (*straight arrow*) originating from left ventricle (LV) and right ventricle (RV), overlying small ventricular septal defect (*arrowhead*). In addition, there is small pericardial effusion (*curved arrow*).
B, Doppler in outflow tract shows common arterial trunk (*straight arrow*) originating from ventricles. Admixture of flow is seen in ventricular septal defect (*arrowhead*). Curved arrow indicates small pericardial effusion.

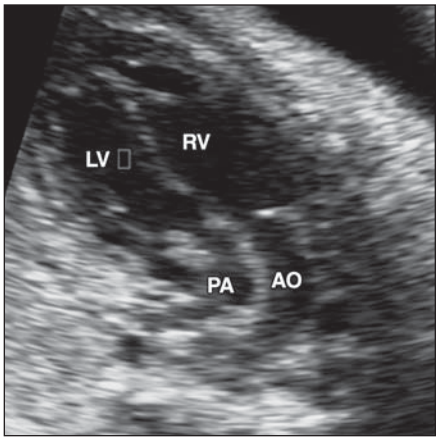

Fig. 11—D-transposition of great arteries. Outflow view shows aorta (AO) and pulmonary artery (PA) parallel to each other, with AO originating from right ventricle (RV) and PA from left ventricle (LV).

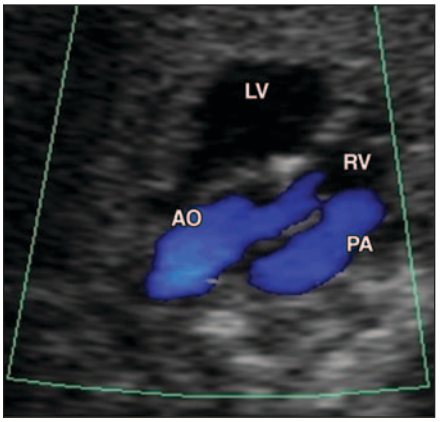

Fig. 12—Double outlet right ventricle. Right ventricular outlet view shows aorta (AO) and pulmonary artery (PA) originating from right ventricle (RV). LV = left ventricle.

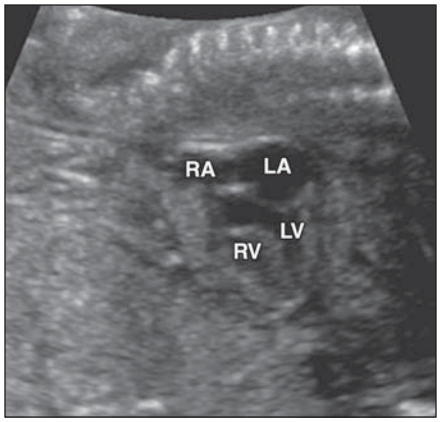

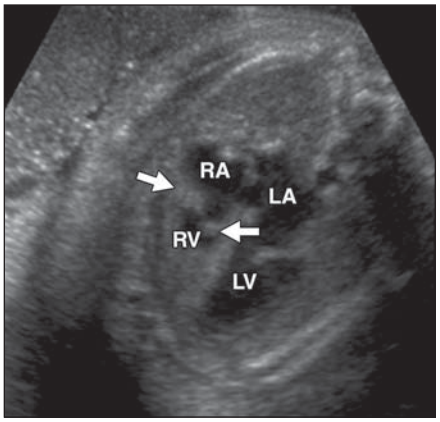

Fig. 13—Right-sided abnormalities.
A, Four-chamber view shows small right ventricle (RV), with normal sized left ventricle (LV), consistent with hypoplastic right heart syndrome. LA = left atrium, RA = right atrium.
B, Four-chamber view show thickened leaflets of tricuspid valve (*arrows*), with restricted opening, consistent with tricuspid stenosis.

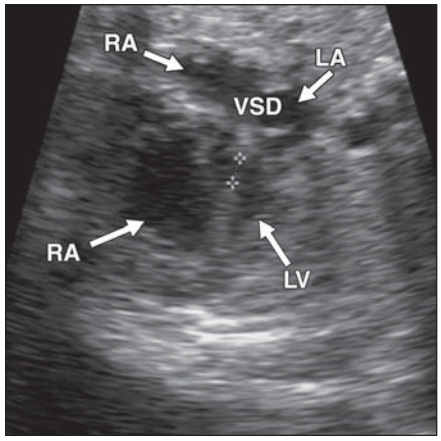

Fig. 14—Hypoplastic left heart syndrome. Four-chamber view shows small left ventricle (LV) and left atrium (LA), associated with ventricular septal defect (VSD) consistent with hypoplastic left heart syndrome. RA = right atrium, RV = right ventricle.

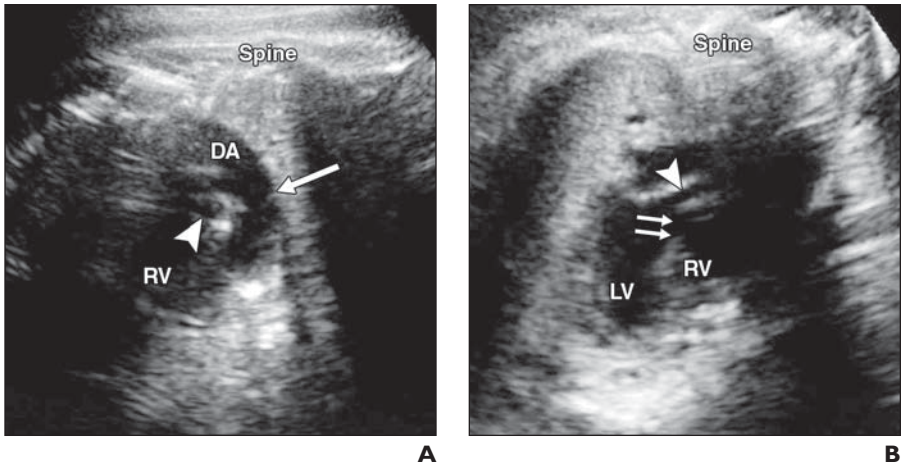

Fig. 15—Hypoplastic aorta.
A, Axial image shows normal size of pulmonary artery (*arrow*) with severe hypoplasia of aorta (*arrowhead*). DA = ductus arteriosus, RV = right ventricle.
B, Another axial image shows severe hypoplasia of aorta (*arrowhead).* In addition, there is ventricular septal defect (*arrows*) that allows flow from left ventricle (LV) to RV.

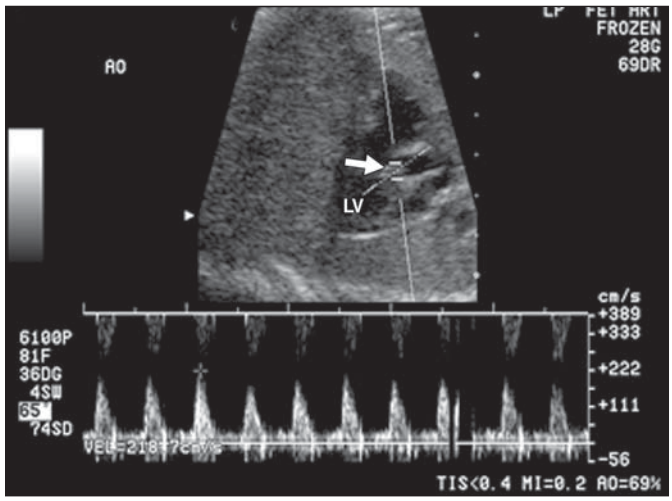

Fig. 16—Aortic stenosis. Doppler through aortic valve reveals increased systolic velocity (*arrow*), with maximal velocity of 218 cm/s, indicative of severe aortic stenosis. LV = left ventricle.

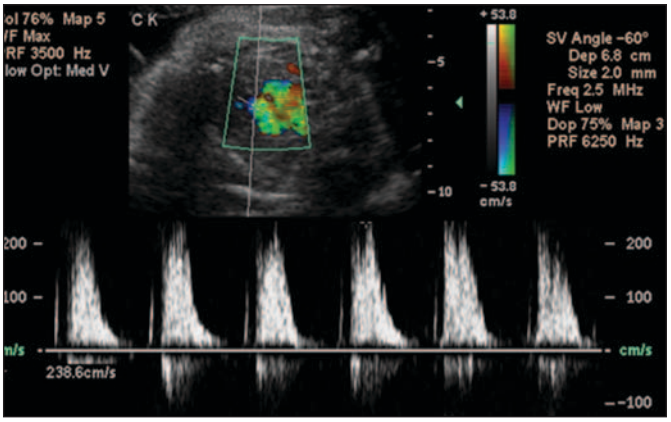

Fig. 17— Pulmonary stenosis. Color Doppler through pulmonary valve reveals increased systolic velocity, with maximal velocity of 240 cm/s, indicative of severe pulmonary stenosis.

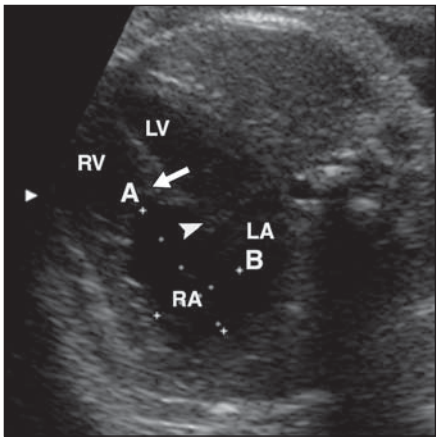

Fig. 18—Ebstein anomaly. Four-chamber view shows apical displacement of tricuspid valve (*arrow*) from level of annulus (*arrowhead*) with severe dilation of right atrium (RA), consistent with Ebstein anomaly. A and B indicate measurement of right atrium, LA = left atrium, LV = left ventricle, RV = right ventricle.

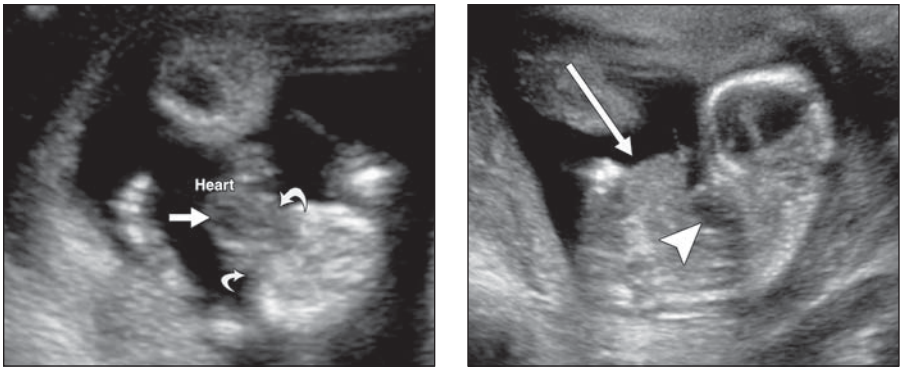

Fig. 19—Pentalogy of Cantrell.
A, Sagittal ultrasound through uterus shows defect in chest wall (*curved arrows*) with heart lying outside thoracic cavity (*arrow*).
B, Patient also had omphalocele (*arrow*) and diaphragmatic hernia (*arrowhead*) consistent with pentalogy of Cantrell.

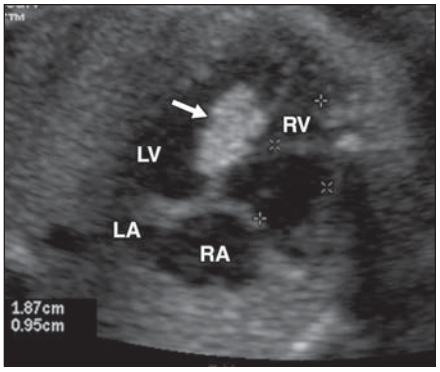

Fig. 20—Cardiac rhabdomyoma. Four-chamber view shows echogenic mass (*arrow*) attached to interventricular septum, in patient with tuberous sclerosis, consistent with rhabdomyoma. LA = left atrium, LV = left ventricle, RA = right atrium, RV = right ventricle.

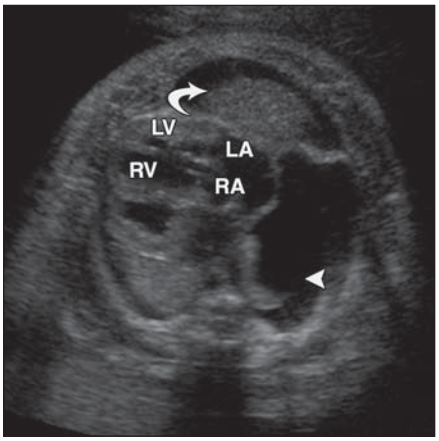

Fig. 21—Dilated cardiomyopathy. Axial view through fetal thorax shows severely dilated heart with dilation of all chambers. In addition, there is pleural effusion (*arrowhead*) and diaphragmatic hernia (*curved arrow*). LA = left atrium, LV = left ventricle, RA = right atrium, RV = right ventricle.

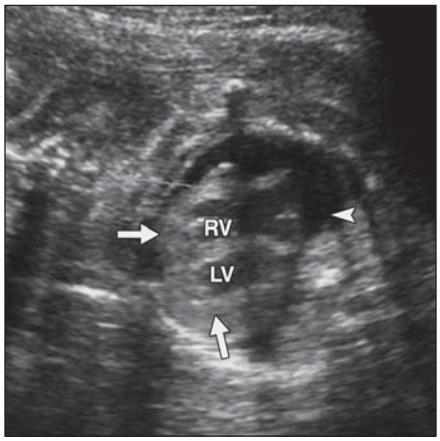

Fig. 22—Hypertrophic cardiomyopathy. Four-chamber view shows severe hypertrophy (*arrows*) of left ventricle (LV) and right ventricle (RV). There is also moderate pericardial effusion (*arrowhead*).

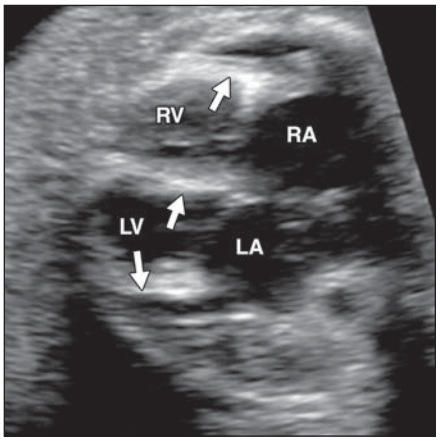

Fig. 23—Endocardial fibroelastosis. Four-chamber views show increased echogenicty (*arrows*) within myocardium of left ventricle (LV) and right ventricle (RV) in patient with endocardial fibroelastosis. LA = left atrium, RA = right atrium.

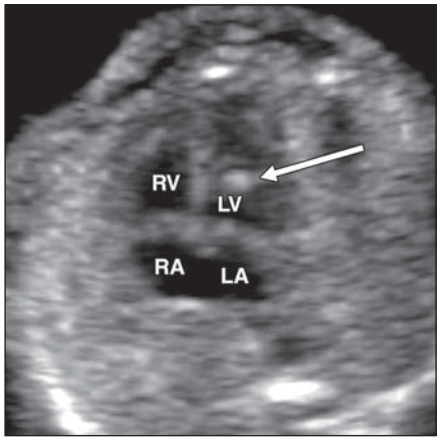

Fig. 24—Echogenic intracardiac foci. Four-chamber view shows echogenic focus (*arrow*) within myocardium. LA = left atrium, LV = left ventricle, RA = right atrium, RV = right ventricle.

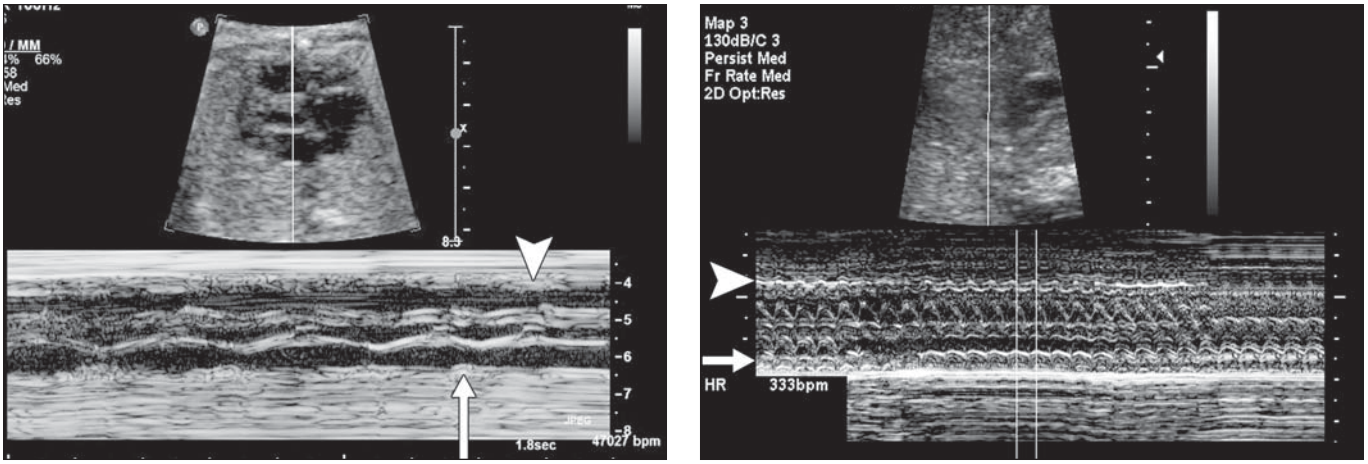

Fig. 25—Fetal arrhythmia.
A, M-mode Doppler images show premature atrial contraction (*arrow*) with subsequent early ventricular contraction (*arrowhead*).
B, M-Mode Doppler images show supraventricular tachycardia—atrial heart rate (*arrowhead*) is fast as well as ventricular heart rate (*arrow*).

FOR YOUR INFORMATION

This article is available for CME credit. See www.arrs.org for more information.